scientific reports

OPEN

Improvement of the froth flotation of LiAlO₂ and melilite solid solution via pre-functionalization

Hao Qiu[1], Jule Kersebaum[1], Annett Wollmann[2], Niklas Feuge[3], Andrea Haas[1], Daniel Goldmann[1✉] & René Wilhelm[3✉]

In this work froth flotation studies with LiAlO₂ (lithium-containing phase) and Melilite solid solution (gangue phase) are presented. The system was optimized with standard collectors and with compounds so far not applied as collectors. Furthermore, the principle of self-assembled monolayers was introduced to a froth flotation process for the first time resulting in excellent yields and selectivities.

With the development and extension of lithium-ion batteries, electric vehicles, the demand for Lithium resources is significantly increasing. In the end market, the share of lithium consumption for batteries increases from 65% in 2019 to 71% in 2020[1–3]. In 2020, the worldwide consumption of lithium content was estimated to 56,000 Tons[2]. With the current growth rate, a potential shortage of raw materials could threaten supply safety. Hence, efficient recovery of lithium from spent LIBs is vital.

Pyrometallurgical processing is one of the vital routes to recycle value metals from spent LIBs with the advantage that input materials can fluctuate[4]. The Umicore Battery Recycling Process is a pyrometallurgical process developed to recover NiMH and spent lithium-ion batteries[5]. Co, Ni, and Cu can be enriched in alloys while Li is transferred into slags[5]. From the composition of a Umicore slag mainly based on the Li₂O–MgO–Al₂O₃–SiO₂–CaO slag system with high aluminum content, it is observed that Li is present in the slag in the form of the LiAlO₂[6]. LiAlO₂ contains about 10% lithium, while the critical lithium-bearing mineral Spodumene contains only 3.7% lithium. Besides, Spodumene needs to be converted from α-Spodumene to β-Spodumene by roasting in the subsequent hydrometallurgical processing, a process that requires substantial amounts of energy[7]. The hydrometallurgical processing of LiAlO₂ enriched silicate slag has also shown that Li recovery can reach 80–95%[5]. Therefore, in comparison, LiAlO₂ is more economically advantageous.

Among several known lithium-containing slags based on the Li₂O–MgO–Al₂O₃–SiO₂–CaO slag system, LiAlO₂ is present in the slags as a lithium-bearing phase[4,6,8]. Melilite solid solution (Melilite s.s.) also appears in the slags as a gangue mineral[4,6]. As a typical slag mineral, its two common end members, gehlenite (Ca₂Al(AlSi)O₇) and åkermanite (Ca₂MgSi₂O₇), which belongs to the melilite group, often forms a continuous solid solution[9–13]. Since LiAlO₂ is a critical lithium-bearing phase in lithium-bearing slag, a systematic study of the floatability of LiAlO₂ and its common gangue minerals in lithium-bearing slags is crucial for the improvement of the pyrometallurgical recovery path for lithium-ion batteries[8]. Previous research has shown that LiAlO₂ can be floated by certain fatty acids (Clariant, Flotinor FS-2 and FS-100) and a phosphoric acid ester (Clariant, Flotinor SM-15)[14]. However, in the real slag, both the lithium yield (approx.60%) and the enrichment factors (approx. 1.5) were insufficient[14].

Froth flotation is based on the selective interaction of collectors with surfaces of different minerals. This adsorption of the collectors can occur via physisorption or chemisorption[15]. It is possible to state that during froth flotation in situ functionalization via physisorption and chemisorption occurs, which is selectively increasing the hydrophobicity of different minerals surfaces. Besides van der Waals interactions and hydrogen bonds[16], electrostatic forces are the predominant cause of physical adsorption[17] of collectors in froth flotation[18]. The formation of a dative bond between a collector and a metal ion is the reason for chemisorption[19], assuming that the stability constants of the "complexes" on the surface in aqueous solution are very far on the product side or the complexed area has become inert due to hydrophobic repulsion of water. In addition, during the froth flotation in water an electrical charge equilibrium is formed[20,21] and different oxides and silicate minerals are partially dissolved,

¹Institute of Mineral and Waste Processing, Waste Disposal and Geotechnics, Clausthal University of Technology, Walther-Nernst-Str. 9, 38678 Clausthal-Zellerfeld, Germany. ²Institute of Particle Technology, Clausthal University of Technology, Leibnizstr. 19, 38678 Clausthal-Zellerfeld, Germany. ³Institute of Organic Chemistry, Clausthal University of Technology, Leibnizstr. 6, 38678 Clausthal-Zellerfeld, Germany. ✉email: daniel.goldmann@tu-clausthal.de; rene.wilhelm@tu-clausthal.de

	Sum (%)
Na_2O	0.2
MgO	4.1
Al_2O_3	15.99
SiO_2	27.49
P_2O_5	0.02
Cl	0.08
K_2O	0.02
CaO	31.88
TiO_2	0.409
MnO	0.04
Fe_2O_3	3.06

Table 1. Chemical composition of Melilite s.s.

resulting in a change of the pH and a "fresh surface" where metal ions may be coordinated by water molecules or by collector molecules via formation of dative bonds[21]. Next to collectors and pH values, froth flotation can also be influenced by frothers, modifiers, depressants, and flocculants[22]. Dissolved metallic ions from metal oxides can also influence the outcome of a froth flotation. They can adsorb on the surface of silicates binding to their hydroxy groups and influencing their flotation behavior[20,23]. Although the in situ functionalization in water is highly complex, with various parameters to be considered, froth flotation is an established method for enrichment and separation of different minerals since the end of the nineteenth century[22].

However, there is also another way to increase the hydrophobicity of mineral surfaces. Under ambient conditions, there is always a layer of adsorbed water present on metal oxides, which leads also on metal ion terminated surfaces to the formation of hydroxyl groups[24–26]. Hence, besides a few defect sides on the surfaces, the predominant terminal functional groups on minerals are hydroxyl moeties[27]. This is utilized in the research field of Self-Assembled Monolayers (SAM) where most commonly condensation reactions in organic solvents between linker groups (also called anchoring groups) and the hydroxyl groups of oxide surfaces create covalent bonds[28]. Functionalized materials with a high surface area have a high potential in fields such as drug delivery[29–31], separation[32], sensing[33], nanotechnology[34], or heterogeneous catalysis[3,35,36]. Hence, they have been functionalized for these applications with different molecules. Taking the latter into account, we present here an alternative approach towards froth flotation and compare the behavior of different collectors in an in situ standard flotation to a pre-functionalization approach.

Experimental details

Materials. Sodium oleate (Riedel-de-Haën), naphthenic acid (Fluka), pine oil (American Cyanamid), bis(2-ethylhexyl) phosphate, dodecyl phosphonic acid (TCI), dibutyl phosphate (Sigma-Aldrich), thenoyltrifluoroacetone (TCI), and trioctyl phosphine oxide (Sigma-Aldrich) were purchased. Naphthenic acid is saponified by adding NaOH to obtain sodium naphthenate. Decyl dihydrogen phosphate[37] was prepared according to literate procedures. $LiAlO_2$ (Sigma-Aldrich) and Melilite s.s. were separately used for flotation experiments. The melilite s.s. ore was obtained from Vata de Sus, located in Hunedoara, Romania. It was firstly crushed with a hammer, then ground in a rod mill, and screened in a stainless-steel screen. The under the size of 63 μm sieve product was selected for flotation tests. $LiAlO_2$ was also sieved, and the under the size of 63 μm sieve product was selected for flotation tests. BET measurements revealed that the sieved $LiAlO_2$ had a BET surface of < 1 m²/g and Melilite s.s. of 3.5 m²/g. X-ray powder diffraction measurement and chemical analysis were performed on the mineral samples. The chemical composition was listed in Table 1. According to XRD analysis, the main phase of the ore is Melilite s.s., and also, there are some impurities such as Merwinite, Wollastonite and Calcite.

Analysis. ATR-IR-Spectra were recorded on an Alpha-T IR (Bruker) with a platinum ATR-unit and diamond crystal. Vibrations are given in cm⁻¹.

Flotation. The flotation test was performed using a modified Hallimond tube (Fig. 1), consisting of three parts: the upper part, the extended part, and the bottom part, produced by HI-ALOQUIMICA, Brazil. All three parts can be freely disassembled for easy cleaning. A piece of porous glass (medium-pore fritted glass) is installed in the bottom part, through which the airflow can enter the tube. A small magnetic stir bar can be placed at the bottom of the Hallimond tube to stir the slurry. The sample amount for each test was 2 g, and the test was carried out at ambient temperature with pine oil (150 g/t) as frother. Firstly, the slurry was mixed and stirred in a beaker for 1 min before the dosing, followed by 1 min after dosing for conditioning. Then the slurry was transferred to Hallimond tube for flotation. The flotation time lasted for 3 min. The airflow rate of each test was controlled to be 1.89 L/h, and the rotation speed was controlled to be 500 rpm. The pretreated samples were not added with collectors. Since $LiAlO_2$ is hydrolyzed in water, its natural pH is about 11. In the meantime, $LiAlO_2$ continuously reacts with sulfuric acid to generate lithium sulfate, making it difficult to adjust the pH to a stable state. Therefore, in this study, the pH value was stabilized using the Britton-Robinson buffer, which con-
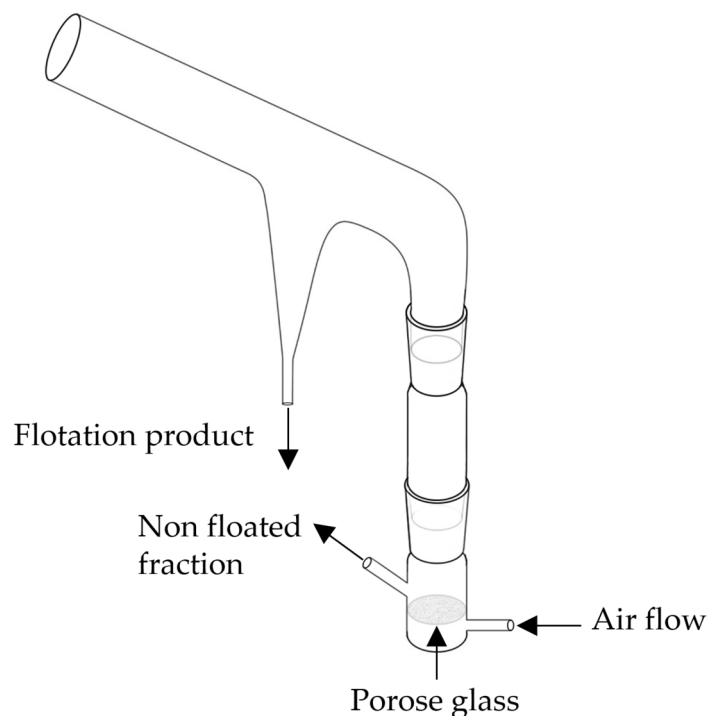
Figure 1. Sketch of the modified Hallimond tube.

sisted of 0.04 M boric acid, 0.04 M phosphoric acid, and 0.04 M acetic acid, and the required pH was achieved by the addition of 0.2 M NaOH.

General functionalization. $LiAlO_2$ or Melilite s.s., 10 w% of organic compound and toluene were refluxed under N_2 in a Dean–Stark apparatus for 16 h or stirred at room temperature for 16 h. Thereafter, the toluene was filtered from the solid. The remaining solid was washed three times with toluene and dried under high vacuum. The combined toluene solutions were evaporated and non-reacted organic compounds were recovered.
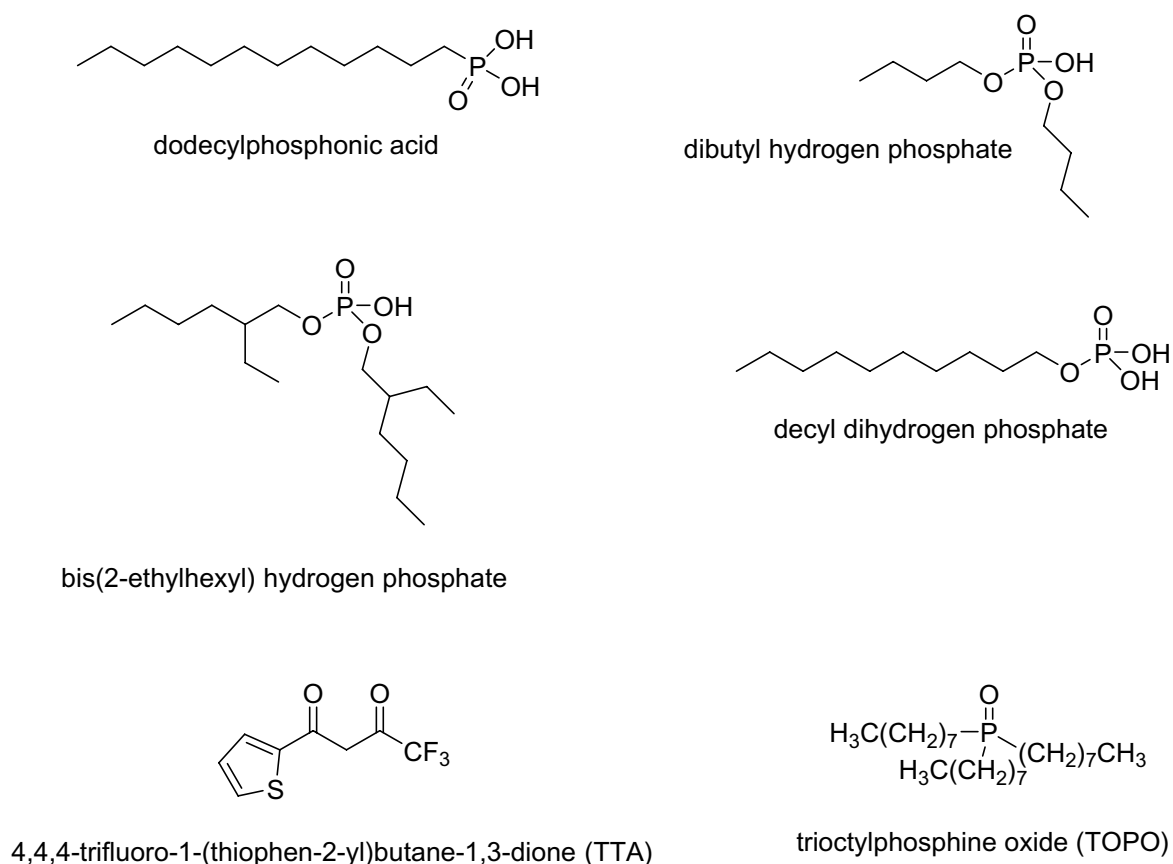
Results and discussion

The investigation started with the functionalization of $LiAlO_2$ as the lithium containing phase and Melilite s.s. as the gangue phase. Each functionalized material was applied in froth flotation and, where possible, compared with the in situ process. Next to sodium oleate further known collectors and compounds, which have not been explored as collectors so far, were used in the froth flotation and are depicted in Fig. 2.
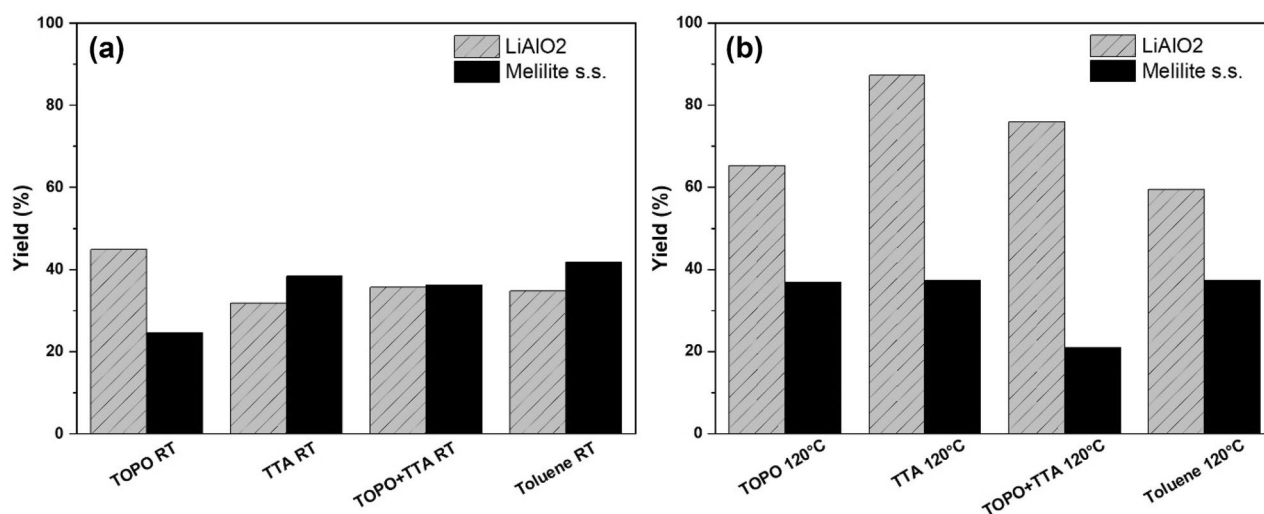
Alkyl phosphonic acids like dodecyl phosphonic acid have been applied for surface functionalizations as self-assemble layers[28] in order to obtain organic electronics[38], material for liquid chromatography[39], to immobilized catalysts[40], or to protect different surfaces of metal oxides[41–44]. A collection of possible types of attachment to oxide surface is shown in Scheme 3[34]. In one case where dodecyl phosphonic acid was applied for the passivation of aluminum and its alloys the quality of the linker group was tested by pH-dependent floating tests[45]. Phosphonic acids are moisture-stable and easy to handle. They have nowadays become standard linkers for various oxidic support materials[46,47]. On the other hand, alkyl phosphonic acids have not been used as collectors in froth flotation. Collectors based on esters of phosphoric acids are well established[48–51].

For pre-functionalized samples, no collector was added in the flotation studies. For comparison a standard froth flotation was optimized for $LiAlO_2$ and Melilite s.s. using sodium oleate (300 g/t) as the best collector resulting in 69% for $LiAlO_2$ and 34% for Melilite s.s. compared to a flotation without a collector, which obtained $LiAlO_2$ in 18% and Melilite s.s. in 16%. Best results achieved under natural pH (For further results in different collector dosages and pHs see Supplementary Information page S2). $LiAlO_2$ and Melilite s.s. were functionalized with 10 w% dodecyl phosphonic acid and n-dibutyl phosphate once in refluxing toluene and once just by stirring at room temperature[40]. After filtration, the material was washed with toluene and dried. The combined toluene filtrates were combined and evaporated to dryness to recover the phosphonic acid or phosphate. In all cases both minerals became very hydrophobic to such an extent that froth flotation experiments were not possible. Nevertheless, the experiments showed that also at room temperature, a high level of functionalization is feasible.

Next, we chose thenoyltrifluoroacetone (TTA) and trioctyl phosphine oxide (TOPO) for the functionalization. TTA is very well known as a complexing agent for extractions[52] including lithium ions[53,54] and as a ligand in various metal complexes[55,56]. It was also used in the surface modification of europium salts[57], but not as a collector in froth flotations. TOPO was applied in the extraction of lithium ions in combination of TTA[54] and other ligands[58]. In addition, it was utilized to functionalize, synthesize, and stabilize perovskite nanomaterial and influencing their band gaps[59–61]. The results of the flotation experiments are shown in Fig. 3. The flotation

dodecylphosphonic acid

dibutyl hydrogen phosphate

bis(2-ethylhexyl) hydrogen phosphate

decyl dihydrogen phosphate

4,4,4-trifluoro-1-(thiophen-2-yl)butane-1,3-dione (TTA)

trioctylphosphine oxide (TOPO)

**Figure 2.** Used collector compounds next to sodium oleate.

Figure 3. Flotation yield of TTA and TOPO functionalized $LiAlO_2$ (**a**) and Melilite (**b**).

yield of $LiAlO_2$, functionalized with TTA at 120 °C, increased to 87% and to 37% for Melilite s.s. The yield of $LiAlO_2$ can be increased to 76% and that of Melilite s.s. to 21% if the functionalization is carried out with a 1:1 mixture of TOPO and TTA. The flotation yields and selectivities in most cases decreased significantly when a functionalization was attempted at room temperature.

It is not possible to compare TTA, TOPO or dodecyl phosphonic acid with a standard froth flotation system and apply them as collectors since they are solids and almost insoluble in water. Hence, sodium oleate was applied in the functionalization experiments in refluxing toluene which provided a yield in the flotation for $LiAlO_2$ of 62%, and for Melilite s.s. of 21% (see Supplementary Information page S18, Figure S25). These results
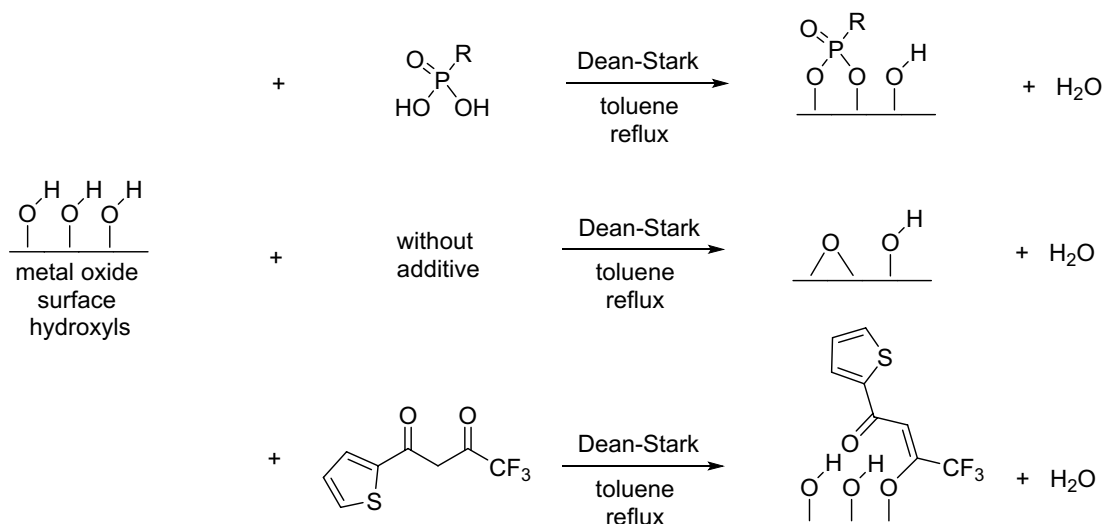
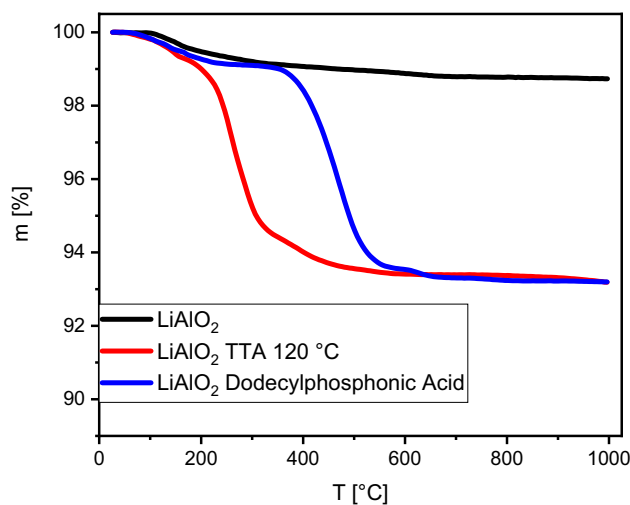**Figure 4.** Functionalization with $LiAlO_2$ and Melilite s.s.
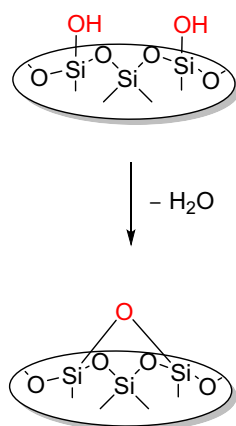
Figure 5. Self-dehydroxylation on silica under water removing.

are slightly off target compared to the standard process. It is reasonable to assume that this is due to desorption of the carboxylate in water. The functionalization with the carboxylate salt primarily proceeds via formation of hydrogen bonds. To form ester bonds the free carboxylic acid is needed[62].

In Fig. 4, some suggestions are given for possible functionalization modes leading to surfaces with enhanced hydrophobicity, which correlates to the flotation yield. Figure 3 shows that the flotation yield of primarily $LiAlO_2$ already increases by just refluxing the material in toluene in a Dean-Stark apparatus. The expected surface reaction is given in Fig. 4 and in more detail in Fig. 5.

It is well known for silica that a self-condensation (i.e. self-dehydroxylation) can occur under water-removing conditions and that this new surface only reacts slowly (weeks) with moisture back to its original structure[63]. This new surface, however, can participate only as a passive partner in a hydrogen bond, hence, the surface is less hydrophilic compared to a surface with hydroxyl groups. It is possible to argue that the increase of the yield of the TTA functionalized material is just adding up to the yield of a dehydroxylated surface. However, from TGA measurements shown in Fig. 6, it is possible to calculate a high loading of TTA molecules on $LiAlO_2$. The loading level was confirmed with elemental analysis results. TGA measurements with Melilite s.s. were not possible due to the high water content of the silicate, hence also elemental analysis was carried out for functionalized $LiAlO_2$ and Melilite s.s. In the case of $LiAlO_2$, elemental analysis results were consistent with TGA studies, and in all cases, $LiAlO_2$ showed a much higher level of functionalization than Melilite s.s. (For further details on TGA and Elemental analysis results, see Supplementary Information, page S7). The proposed structure of TTA on $LiAlO_2$ in Fig. 4 would also occur when TTA is reacting with the quasi-condensed epoxide-type surface. The TGA measurements of dodecyl phosphonic acid are in very good agreement with the literature[64], where first the bond between the phosphorous atom and the alkyl chain is cleaved. Also, the presence of one covalent bond for TTA is supported by the TGA results.

FT-IR measurements were also conducted to get further inside on the level of functionalization of each material. As can be seen in Fig. 7, the signals of TTA are found in the functionalized material. The signals are

**Figure 6.** Selected TGA measurements of functionalized LiAlO$_2$ conditions[63].
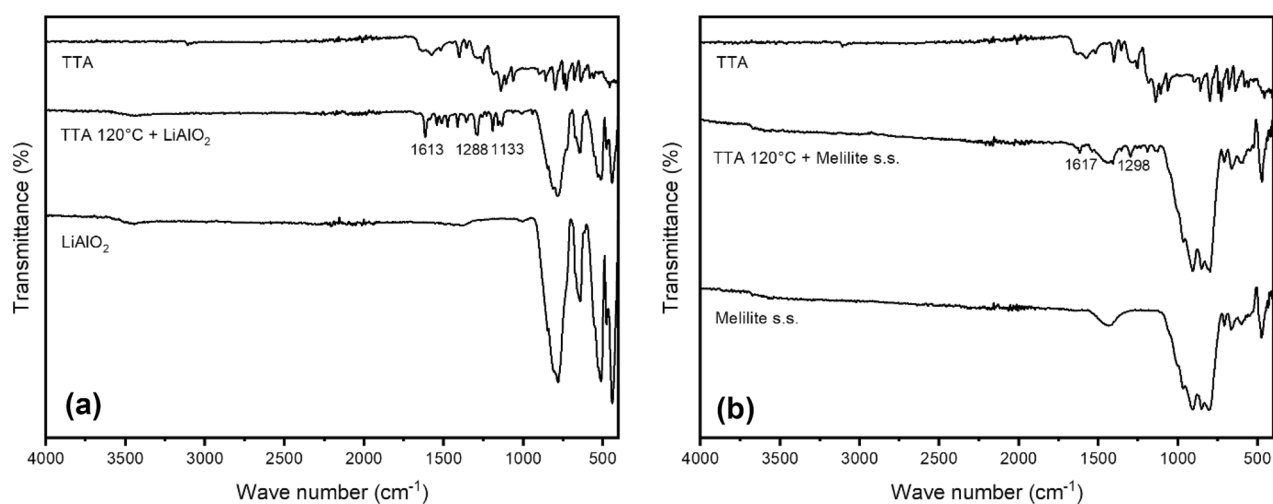
**Figure 7.** FT-IR measurement of TTA functionalized LiAlO$_2$ (**a**) and Melilite s.s. (**b**).

significantly stronger with LiAlO$_2$ as with Melilite s.s. Taking into account the unfavorable ratio of the surface to the rest of the material the FT-IR spectra are not intensive enough to prove the exact mode of functionalization as suggested in Fig. 4. However, this is in the field of SAM for bulk material a common phenomenon[40]. Yet, the presence of sharp peaks at the functionalized material compared to TTA suggest that a strong ordered functionalization took place. (For further FT-IR spectra see Supplementary Information, page S9).

Considering that phosphorous esters and phosphonic acids resulted into functionalized material too hydrophobic for froth flotation studies, decyl dihydrogen phosphate and bis (2-ethylhexyl) phosphate were investigated under standard froth flotation conditions using the Hallimond tube. Decyl dihydrogen phosphate (Fig. 2) can be simply prepared from decanol and phosphorus oxylchloride[37]. It is used as extractant[65], and there are just limited reports where it was applied in the flotation cassiterite[48] and manganese based ores[49]. Bis(2-ethylhexyl) phosphate (Fig. 2) has a large van der Waals Radius around the phosphate moiety due to its two-branched alkyl moieties. This and the fact that only one acidic hydroxy group at the phosphate moiety remains could influence the interaction of the molecule with different ores. Bis(2-ethylhexyl) phosphate was extensively applied as an extractant for different metal ions[66,67], including also lithium when applied in combination with tributyl phosphate[68]. In addition, some calcium minerals and sphalerite have been investigated with bis(2-ethylhexyl) phosphate in flotation experiments[50,51]. However, with lithium-containing minerals so far flotation experiments with these collectors, have not been reported so far.

The effect of collector dosage on the flotation of LiAlO$_2$ and Melilite s.s. with decyl dihydrogen phosphate is shown in Figs. 8 and 9 at ambient temperature and at natural pH, pH 7, and pH 9. The yield increased slowly with the rise of the collector dosage and reached its maximum (56.03%) at natural pH. Its highest yield is lower than that of the sodium oleate system. This can be explained by considering that decyl dihydrogen phosphate is
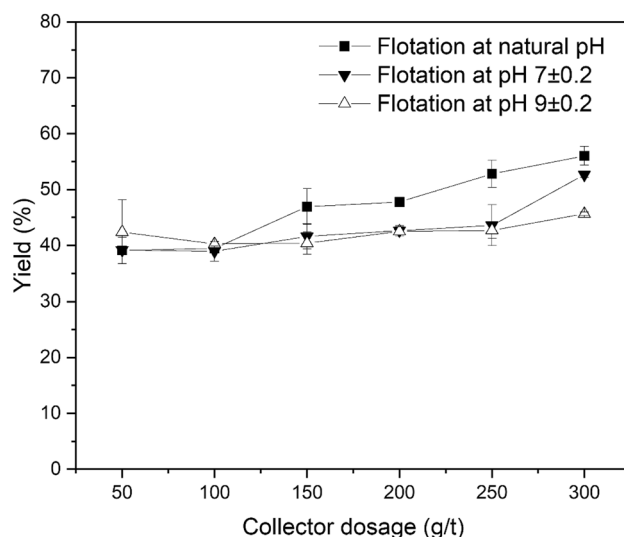
Figure 8. Effect of Collector Dosage on Flotation of $LiAlO_2$ using decyl dihydrogen phosphate.
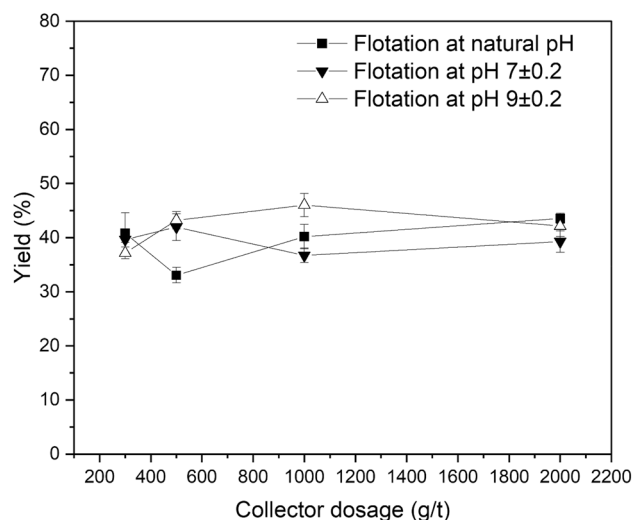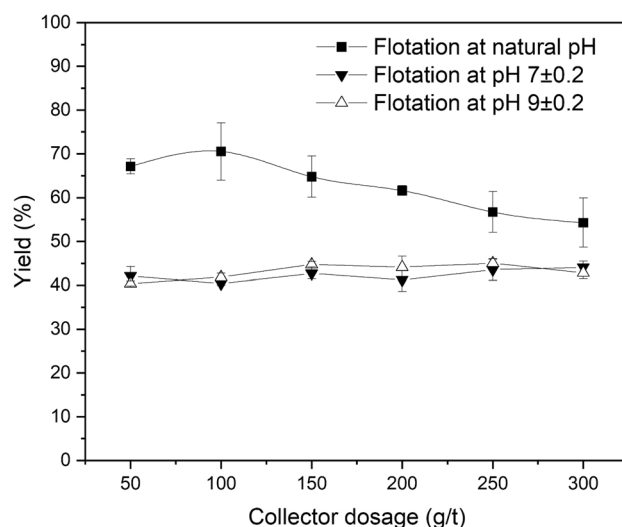

Figure 9. Effect of Collector Dosage on Flotation of Melilite s.s. using decyl dihydrogen phosphate.

a sterical non-hindered phosphoric mono-ester and hydrolysis can occur too fast, resulting in the formation of an alcohol and phosphoric acid.

Figure 9 presents the effects of collector dosage on Melilite s.s. yield in the Hallimond tube flotation with decyl dihydrogen phosphate at ambient temperature and at natural pH, pH 7 and pH 9. Combining Figs. 8 and 9, it is possible to note that for the flotation of $LiAlO_2$, decyl dihydrogen phosphate has a low selectivity. The yield of Melilite s.s. with a dosage of 300 g/t is about 10% lower than that of $LiAlO_2$, which can be explained again by the fast hydrolysis of the collector.

Thereafter the more hindered bis(2-ethylhexyl) phosphate was investigated. It was assumed that the hydrolysis rate is low enough to be applicable for the time frame during the experiment was conducted. Figure 10 presents the effects of collector dosage on $LiAlO_2$ yield in the Hallimond tube flotation with bis(2-ethylhexyl) phosphate at ambient temperature and at natural pH, pH 7 and pH 9. At natural pH, the yields of $LiAlO_2$ were above 60% in the first two experiments, demonstrating excellent floatability. However, in subsequent repeated experiments, one month after the first experiments, the recovery decreased to some extent. This may be related to the slow hydrolysis of the phosphate, which was stored in a ready to use aqueous solution for over a month for the experiments. In the flotation experiments at pH 7 and pH 9, the yields were very close and did not show significant changes with increasing agent dosage.

Figure 11 presents the effects of collector dosage on Melilite s.s. yield in the Hallimond tube flotation with bis (2-ethylhexyl) phosphate at ambient temperature and at natural pH, pH 7 and pH 9. Combining Figs. 10 and 11, it is possible to see that for the flotation of $LiAlO_2$, bis (2-ethylhexyl) phosphate has a certain selectivity. The collector showed an excellent recovery of $LiAlO_2$ and a good selectivity.

Figure 10. Effect of Collector Dosage on Flotation of $LiAlO_2$ using bis(2-ethylhexyl) phosphate at natural pH, pH 7 and pH 9.
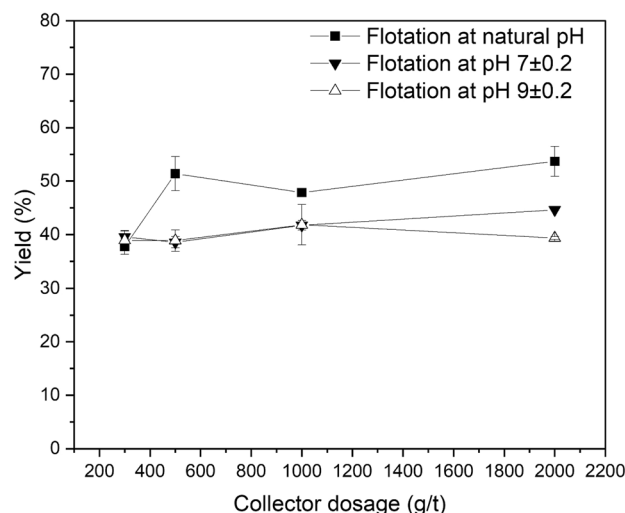
Figure 11. Effect of Collector Dosage on Flotation of Melilite s.s. using bis(2-ethylhexyl) phosphate.

Collector dosage of sodium oleate (g/t)	Yield of $LiAlO_2$ (%)	Yield of Melilite s.s. (%)
150	60.32	2.88
300	91.61	7.64

Table 2. Optimized Froth Flotation with a standard collector in a small flotation machine (Denver) and pine oil (150 g/t) as frother.

Finally, a standard system was also scaled up in a small flotation machine. The achieved results are shown in Table 2 for $LiAlO_2$ and Melilite s.s. at natural pH by using a small flotation machine.

The IR-spectra of $LiAlO_2$, sodium oleate, and $LiAlO_2$ treated in 10^{-5} M sodium oleate solution are given in Fig. 12a. The bands at 1422 cm^{-1} and 1559 cm^{-1} are attributed to the symmetric and asymmetric stretching vibration of –COO– for the sodium oleate[69]. After treated with sodium oleate, the IR-spectra of $LiAlO_2$ displays a new band at 1378 cm^{-1}. The desorption experiment was also carried out. The new band at 1378 cm^{-1} in IR-Spectra did not disappear after strong stirring in sodium oleate solution and washing with distilled water, as shown in Fig. 12b. The appearance of this new band indicates the possibility of the formation of aluminum oleate. However, the IR measurements cannot completely display the behavior in the solution state. (For further FT-IR spectra see Supplementary Information, page S9) Contact angle measurements (Washburn) were also performed on
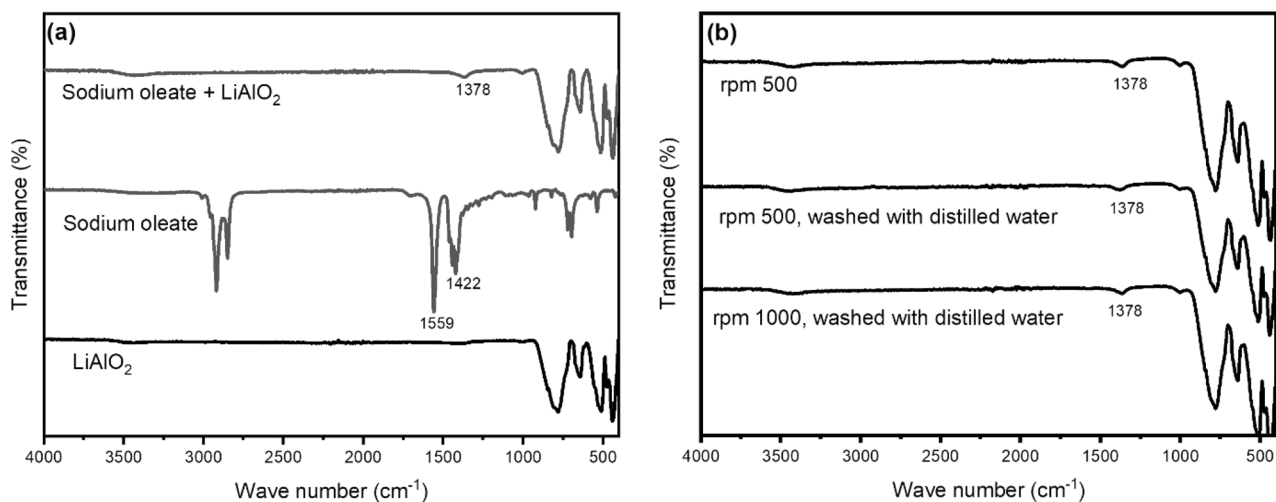
Figure 12. (**a**) IR spectra of LiAlO$_2$, Sodium oleate and LiAlO$_2$ treated in sodium oleate solution. (**b**) IR spectra of samples obtained after the desorption experiment: stirred at a rate of 500 rpm without washing; stirred at 500 rpm with washing; stirred at 1000 rpm with washing.
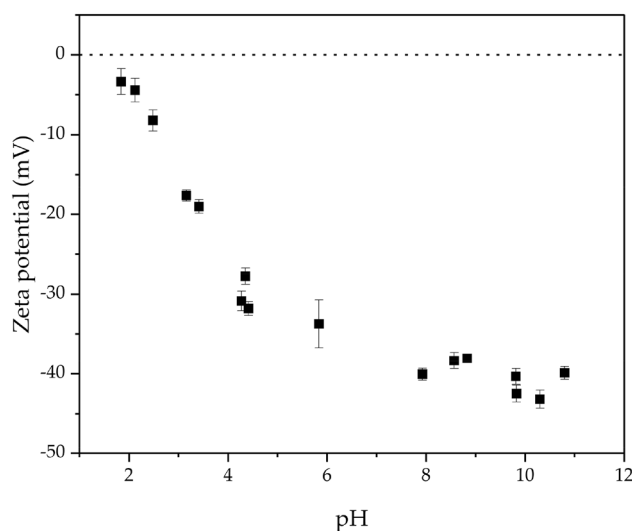
Figure 13. Zeta potential of Melilite s.s.

LiAlO$_2$. The contact angle of untreated LiAlO$_2$ is 27.99°, while the contact angle increased to 89.49° after the addition of sodium oleate.

In the sodium oleate system, the overall yield of Melilite s.s. is lower than that of LiAlO$_2$. As shown in Fig. 13, the Zeta potential of Melilite s.s. indicates that under our experimental conditions, the zeta potential remains negative throughout the pH range (from pH 2 to pH 11), and never reaches its point of zero charge (PZC). This result is also similar to the measurement of synthetic gehlenite measured by Udaeta et al.[70] (for further details on Zeta potential measurement see Supplementary Information, page S18). From the point of view of surface potential, sodium oleate may not be electrostatically adsorbed on Melilite s.s.. Meanwhile, new peaks for oleate adsorption were not observed during IR measurements (see Supplementary Information, page S9).

Conclusion

In summary it was possible to show that LiAlO$_2$ and Melilite s.s. are separable in a froth flotation. Both standard collectors and compounds not previously used as collectors were investigated. Very good yields and selectivities could be achieved with these collectors after optimization. Furthermore, the principle of self-organized monolayers (SAM) was introduced for the first time in a froth flotation system. The pre-functionalization resulted in a significant improvement compared to the standard. These results will allow a new approach for the separation of different minerals via froth flotation in the future and further studies are currently conducted.

References

1. Jaskula, B. W. Lithium. https://pubs.usgs.gov/periodicals/mcs2020/mcs2020-lithium.pdf (2020).
2. Jaskula, B. W. Lithium. https://pubs.usgs.gov/periodicals/mcs2021/mcs2021-lithium.pdf (2021).
3. Lin, Z., Shen, S., Wang, Z. & Zhong, W. Laser ablation in air and its application in catalytic water splitting and Li-ion battery. *iScience* **24**, 102469 (2021).
4. Schirmer, T., Qiu, H., Li, H., Goldmann, D. & Fischlschweiger, M. Li-distribution in compounds of the Li_2O-MgO-Al_2O_3-SiO_2-CaO system—A first survey. *Metals* **10**, 1633 (2020).
5. Elwert, T., Goldmann, D., Schirmer, T. & Strauß, K. in *Recycling und Rohstoffe* 679–690 (2012).
6. Elwert, T., Strauss, K., Schirmer, T. & Goldmann, D. Phase composition of high lithium slags from the recycling of lithium ion batteries. *World Metall Erzmetall* **65**, 163–171 (2012).
7. Welham, N. J. in *SME Mineral Processing and Extractive Metallurgy Handbook* (eds R. C. Dunne, S. K. Kawatra, & C. A. Young) 1840 (Society for Mining, Metallurgy & Exploration, 2019).
8. Wittkowski, A., Schirmer, T., Qiu, H., Goldmann, D. & Fittschen, U. E. A. Speciation of manganese in a synthetic recycling slag relevant for lithium recycling from lithium-ion batteries. *Metals* **11**, 188 (2021).
9. Engström, F., Adolfsson, D., Samuelsson, C., Sandström, Å. & Björkman, B. A study of the solubility of pure slag minerals. *Min. Eng.* **41**, 46–52 (2013).
10. Deer, W. A., Howie, R. A. & Zussman, J. *An Introduction to the Rock-Forming Minerals* 3rd edn. (The Minerological Society, 2013).
11. Ren, Y. F. *Metallurgical Process Mineralogy* (Metallurgical Industry Press, 1996).
12. Reddy, A. A. *et al.* Sintering and devitrification of glass-powder compacts in the akermanite–gehlenite system. *J. Mater. Sci.* **48**, 4128–4136 (2013).
13. Stavrakeva, D. & Georgieva, I. New data on the composition of melilite during solid phase and solid-liquid phase synthesis. *Comptes Rendus-Academie Bulgare des Sciences* **48**, 91–94 (1995).
14. Haas, A., Elwert, T., Goldmann, D. & Schirmer, T. in *European Mineral Processing & Recycling Congress.* (ed GDMB) (GDMB Verlag GmbH).
15. Adamson, A. W. *Physical Chemistry of Surfaces* 4th edn. (Wiley, 1982).
16. Hollander, A. F., Somasundaran, P. & Gryte, C. C. in *Adsorption from Aqueous Solutions* (ed P. H. Tewari) (Plenum Press, 1981).
17. Parfitt, G. D. & Rochester, C. H. in *Adsorption from Solution at the Solid/Liquid Interface* (eds G. D. Parfitt & C. H. Rochester) 3 (Academic Press, 1983).
18. Somasundaran, P. & Fuerstenau, D. W. Mechanisms of alkyl sulfonate adsorption at the alumina-water interface. *J. Phys. Chem.* **70**, 90–96 (1966).
19. French, R. O., Wadsworth, M. E., Cook, M. A. & Cutler, I. B. The quantitative application of infrared spectroscopy to studies in surface chemistry. *J. Phys. Chem.* **58**, 805–811 (1954).
20. Ananthapadmanabhan, K. P. & Somasundaran, P. Surface precipitation of inorganics and surfactants and its role in adsorption and flotation. *Colloids Surf.* **13**, 151–167 (1985).
21. Fuerstenau, M. C. in *Flotation—Gaudin Memorial Volume* Vol. 1 (ed M. C. Fuerstenau) 148–196 (AIME, 1976).
22. Fuerstenau, M. C., Miller, J. D. & Kuhn, M. C. *Chemistry of Flotation* (Soc of Mining Engineers of AIME, 1985).
23. Hanna, H. S. & Somasundaran, P. in *Flotation-Gaudin Memorial Volume* Vol. 1 (ed M. C. Fuerstenau) 197 (AIME, 1976).
24. Calò, A., Domingo, N., Santos, S. & Verdaguer, A. Revealing water films structure from force reconstruction in dynamic AFM. *J. Phys. Chem. C* **119**, 8258–8265 (2015).
25. Shen, Y. R. & Ostroverkhov, V. Sum-frequency vibrational spectroscopy on water interfaces: Polar orientation of water molecules at interfaces. *Chem. Rev.* **106**, 1140–1154 (2006).
26. Thissen, P., Grundmeier, G., Wippermann, S. & Schmidt, W. G. Water adsorption on the α-Al_2O_3(0001) surface. *Phys. Rev. B* **80**, 245403 (2009).
27. Hass, K. C., Schneider, W. F., Curioni, A. & Andreoni, W. The chemistry of water on alumina surfaces: Reaction dynamics from first principles. *Science* **282**, 265–268 (1998).
28. Ulman, A. Formation and structure of self-assembled monolayers. *Chem. Rev.* **96**, 1533–1554 (1996).
29. Vallet-Regí, M., Balas, F. & Arcos, D. Mesoporous materials for drug delivery. *Angew. Chem. Int. Ed.* **46**, 7548–7558 (2007).
30. Rosenholm, J. M., Sahlgren, C. & Lindén, M. Towards multifunctional, targeted drug delivery systems using mesoporous silica nanoparticles: Opportunities & challenges. *Nanoscale* **2**, 1870–1883 (2010).
31. Croissant, J. G., Fatieiev, Y., Almalik, A. & Khashab, N. M. Mesoporous silica and organosilica nanoparticles: Physical chemistry, biosafety, delivery strategies, and biomedical applications. *Adv. Healthcare Mater.* **7**, 1700831 (2018).
32. Qiu, H., Liang, X., Sun, M. & Jiang, S. Development of silica-based stationary phases for high-performance liquid chromatography. *Anal. Bioanal. Chem.* **399**, 3307–3322 (2011).
33. Wagner, T. *et al.* A high temperature capacitive humidity sensor based on mesoporous silica. *Sensors* **11**, 3135–3144 (2011).
34. Cattani-Scholz, A. Functional organophosphonate interfaces for nanotechnology: A review. *ACS Appl. Mater. Interfaces* **9**, 25643–25655 (2017).
35. Tüysüz, H. & Schüth, F. Ordered mesoporous materials as catalysts. *Adv. Catal.* **55**, 127–239 (2012).
36. Shen, S. *et al.* Reversed active sites boost the intrinsic activity of graphene-like cobalt selenide for hydrogen evolution. *Angew. Chem. Int. Ed.* **60**, 12360–12365 (2021).
37. Okamoto, Y. Synthesis of alkyl dihydrogenphosphate by the reaction of alcohols and silyl polyphosphate. *Bull. Chem. Soc. Jpn.* **58**, 3393–3394 (1985).
38. Chang, J.-F. *et al.* Enhanced mobility for increasing on-current and switching ratio of vertical organic field-effect transistors by surface modification with phosphonic acid self-assembled monolayer. *Org. Electr.* **81**, 105689 (2020).
39. Song, Z. *et al.* Facile synthesis of zirconia-coated mesoporous silica particles by hydrothermal strategy under low potential of hydrogen conditions and functionalization with dodecylphosphonic acid for high-performance liquid chromatograph. *J. Chromat. A* **1612**, 460659 (2020).
40. Weinberger, C. *et al.* Straightforward immobilization of phosphonic acids and phosphoric acid esters on mesoporous silica and their application in an asymmetric aldol reaction. *Nanomaterials* **9**, 249–260 (2019).
41. Hopmann, E. & Elezzabi, A. Y. Electrochemical stability enhancement of electrochromic tungsten oxide by self-assembly of a phosphonate protection layer. *ACS Appl. Mater. Interfaces* **12**, 1930–1936 (2020).
42. Nicovich, P. R., Lu, X., Gaus, K. & Gooding, J. J. Characterization of functionalized glass and indium tin oxide surfaces as substrates for super-resolution microscopy. *J. Phys. D: Appl. Phys* **52**, 034003 (2019).
43. Wisser, F. M. *et al.* Detection of surface silanol groups on pristine and functionalized silica mixed oxides and zirconia. *J. Colloid Interface Sci.* **374**, 77–82 (2012).
44. Hu, A., Yee, G. T. & Lin, W. Magnetically recoverable chiral catalysts immobilized on magnetite nanoparticles for asymmetric hydrogenation of aromatic ketones. *J. Am. Chem. Soc.* **127**, 12486–12487 (2005).

45. Maege, I. *et al.* Self-assembling adhesion promoters for corrosion resistant metal polymer interfaces. *Prog. Org. Coatings* **34**, 1–12 (1998).
46. Guerrero, G., Alauzun, J. G., Granier, M., Laurencin, D. & Mutin, P. H. Phosphonate coupling molecules for the control of surface/interface properties and the synthesis of nanomaterials. *Dalton Trans.* **42**, 12569–12585 (2013).
47. Pujari, S. P., Scheres, L., Marcelis, A. T. M. & Zuilhof, H. Covalent surface modification of oxide surfaces *Angew. Chem. Int. Ed.* **53**, 6322–6356 (2014).
48. Cheng, J. & Zhio, J. Collecting performances and adsorption mechanism of alkylphosphorous esters on cassiterite. *Youse Jinshu* **38**, 37–43 (1986).
49. Hazen, W. C. Method of beneficiating sulfide and oxide ores of copper, manganese, lead and zinc. USA patent (1962).
50. Filippova, I. V., Filippov, L. O., Duverger, A. & Sererov, V. V. Synergetic effect of a mixture of anionic and nonionic reagents: Ca mineral contrast separation by flotation at neutral pH. *Min. Eng.* **66–68**, 135–144 (2014).
51. Das, B. & Naik, P. K. Electrokinetics, adsorption and flotation studies of sphalerite using di(2-ethyl hexyl)phosphoric acid. *Can. Metall. Q.* **43**, 355–362 (2004).
52. Moghadam, M. R., Haji, A. M. & Dadfarnia, S. S. Spectrophotometric determination of iron species using a combination of artificial neural networks and dispersive liquid–liquid microextraction based on solidification of floating organic drop. *J. Hazard. Mater.* **197**, 176–182 (2011).
53. Itoh, T., Billah, M., Honjo, T. & Terada, K. Separation and determination of a trace amount of lithium as its complex with 12-crown-4 by means of synergic extraction and flame thenoyltrifluoroacetone photometry. *Anal. Sci.* **7**, 47–50 (1991).
54. Zhang, L. *et al.* Solvent extraction of lithium from ammoniacal solution using thenoyltrifluoroacetone and neutral ligands. *J. Mol. Liquids* **274**, 746–751 (2019).
55. Mahesha, *et al.* μ-Phenoxide bridged mixed ligand Cu(II) complex: Synthesis, 3D supramolecular architecture, DFT, energy frameworks and antimicrobial studies. *Polyhedron* **185**, 114571 (2020).
56. de Souza-Furtado, F. A. *et al.* Molecular information on the potential of europium complexes for local recognition of a nucleoside-based drug by using nanostructured interfaces assembled as langmuir–blodgett films. *Langmuir* **36**, 3843–3852 (2020).
57. Yu, L., Gao, J., Zeng, Z. & Zheng, Y. Surface modifcation via 2-thenoyltrifluoroacetone and the photophysical studies. *Chem. Papers* **75**, 873–881 (2021).
58. Masmoudi, A., Zante, G., Trebouet, D., Barillon, R. & Boltoeva, M. Solvent extraction of lithium ions using benzoyltrifluoroacetone in new solvents. *Sep. Purf. Technol.* **255**, 117653 (2021).
59. Zhu, H. *et al.* Enhancing the properties of perovskite quantum dot light emitting devices through grid structures formed by tri-octylphosphine oxide. *J. Mater. Chem. C* **8**, 9861–9866 (2020).
60. Peng, S. *et al.* Effective surface ligand-concentration tuning of deep-blue luminescent FAPbBr 3 nanoplatelets with enhanced stability and charge transport. *ACS Appl. Mater. Interfaces* **12**, 31863–31874 (2020).
61. Baek, S. *et al.* Highly stable all-inorganic perovskite quantum dots using a ZnX2-trioctylphosphine-oxide: Application for high-performance full-color light-emitting diode. *Adv. Optical Mater.* **8**, 1901897 (2020).
62. Newman, M. S. *An Advanced Organic Laboratory Course* Vol. 8 (Macmillan, 1972).
63. Comas-Vives, A. Amorphous SiO_2 surface models: Energetics of the dehydroxylation process, strain, ab initio atomistic thermodynamics and IR spectroscopic signatures. *Phys. Chem. Chem. Phys.* **18**, 7475–7482 (2016).
64. Wan, X. *et al.* Thermal stability of phosphonic acid self-assembled monolayers on alumina substrates. *J. Phys. Chem. C* **124**, 2531–2542 (2020).
65. Hardy, C. J., Greenfield, B. F. & Scargill, D. Solvent extraction of beryllium from aqueous solutions of mineral acids by alkyl esters of phosphoric acid. *J. Chem. Soc.*, 174–182 (1961).
66. Kolarik, Z. & Pankova, H. Acidic organophosphorus extractants: I: Extraction of lanthanides by means of dialkyl phosphoric acids: Effect of structure and size of alkyl group. *J. Inorg. Nucl. Chem.* **28**, 2325–2333 (1966).
67. Erust, C., Akcil, A., Tuncuk, A., Deveci, H. & Yazici, E. Y. A multi-stage process for recovery of neodymium (Nd) and dysprosium (Dy) from spent hard disc drives (HDDs). *Miner. Process. Extr. Metall. Rev.* **42**, 90–101 (2021).
68. Song, Y., Zhao, Z. & He, L. Lithium recovery from Li3PO4 leaching liquor: Solvent extraction mechanism of saponified D2EHPA system. *Sep. Pur. Tech.* **249**, 117161 (2020).
69. Liu, W. *et al.* Flotation behaviors of ilmenite, titanaugite, and forsterite using sodium oleate as the collector. *Min. Eng.* **72**, 1–9 (2015).
70. Udaeta, M. C., Ponou, J., Dodbiba, G. & Fujita, T. Enrichment of silicocarnotite from silicocarnotite and gehlenite mixtures using a kerosene-based liquid-liquid separation process. *J. Environ. Chem. Eng.* **7**, 103387 (2019).

Acknowledgements

Author contributions

H.Q. and J.K. performed the experiments and were responsible for analytical data preparation. A.W. performed TGA measurements. N.F. was preparing Elemental Analysis und TGA data. H.Q. and A.H. prepared the manuscript draft and R.W. wrote the manuscript. D.G. and R.W. supervised all of the work. All authors helped in improving the manuscript.

Funding

Competing interests

The authors declare no competing interests.

Additional information

Supplementary Information The online version contains supplementary material available at https://doi.org/10.1038/s41598-021-00008-z.

Correspondence and requests for materials should be addressed to D.G. or R.W.

Reprints and permissions information is available at www.nature.com/reprints.

Publisher's note Springer Nature remains neutral with regard to jurisdictional claims in published maps and institutional affiliations.